Opto-Electronics Review

Advances in type-II superlattice research at Fraunhofer IAF

Raphael Müller [*], Volker Daumer, Tsvetelina Hugger, Lutz Kirste, Wolfgang Luppold,
Jasmin Niemasz, Robert Rehm, Tim Stadelmann, Mark Wobrock, Quankui Yang

Fraunhofer Institute for Solid State Physics IAF, Tullastraße 72, 79108 Freiburg, Germany

Article info	Abstract
	Current advances in type-II superlattice (T2SL) research at Fraunhofer IAF are elaborated on in this paper. First, the use of metastructures for quantum efficiency (QE) enhancement in the longwave infrared (LWIR) is presented. Finite element modelling results are reported on that suggest a potential for doubling of the QE at certain wavelengths with the investigated device structure. Next, characterisation results of midwave infrared (MIWR) InAs/InAsSb T2SL nBn detectors are shown. The low, diffusion-limited dark current above 120 K and a QE of 60% are comparable to the state-of-the-art. Finally, groundwork for InAs/GaSb T2SL MWIR/LWIR dual-band detector arrays based on a back-to-back heterojunction diode device concept is presented. The dry etching technology allows for steep etch trenches and full pixel reticulation with a fill factor of about 70% at 12 µm pitch. The detector characterisation at 77 K and ±250 mV bias demonstrates the bias-switchable operation mode with dark current densities of $6.1 \cdot 10^{-9}$ A/cm² in the MWIR and $5.3 \cdot 10^{-4}$ A/cm² in the LWIR.

1. Introduction

There is high interest in infrared (IR) material research and development for high performance imaging applications. Type-II superlattices (T2SLs) have established as a competitive alternative to the prevalent HgCdTe technology for the fabrication of focal plane arrays (FPAs). This owes to better producibility, spatial uniformity, temporal stability, and scalability, which ultimately results in lower costs [1]. In the last decade, in particular, research and development efforts in the framework of the US Vista program fostered interest in T2SL technology and demonstrated its potential for application and cost reduction for high performance IR imaging [2].

Since the mid-1990s, T2SLs for IR detection are investigated at Fraunhofer IAF [3, 4]. In recent years, we concentrated on the supply of InAs/GaSb T2SL detector arrays for multi-colour infrared alerting sensors. These arrays, both developed and manufactured at Fraunhofer IAF, enable simultaneous co-located detection

in the 3–4 µm and the 4–5 µm spectral ranges with a format of 384×288 pixels at 40 µm pitch [5].

In current research projects, we set focus on InAs/InAsSb (Ga-free) T2SLs, as well as dual-band imaging, for the midwave infrared (MWIR) and the longwave infrared (LWIR), based on InAs/GaSb T2SLs. Our developments reflect the recent research trends of increasing resolution, reducing the pixel pitch, and rising the operating temperature. The requirements imposed by our developments necessitate the adaption of growth and processing schemes.

In this paper, an overview on recent development efforts devoted to improving T2SL detector performance is presented. First, an approach for quantum efficiency (QE) enhancement in the LWIR employing metastructures is described. Second, initial characterisation results on MWIR InAs/InAsSb nBn detectors are shown. Third and last, the need for steep etch trenches in InAs/GaSb T2SL MWIR/LWIR dual-band detectors with small pixel pitch and high fill factor is elaborated on. Some aspects of the dry etching development are presented, as well as electro-optical characterisation results of the first detector structures.

2. Metastructures for QE enhancement

2.1. Introduction

Conventional LWIR T2SL detectors suffer from a comparably low QE. T2SLs that detect at longer wavelengths require a larger period length, which reduces the oscillator strength, the absorption coefficient and, eventually, the QE. Absorption can be increased by using a detector with a wider absorber layer. The drawback of this approach is, however, that the diffusion length of photogenerated carriers may become a limiting factor preventing the intended QE increase.

A conceptually different way to enhance detector QE is employing a stronger coupling between the incoming radiation field and the detector. Figuratively, the aim is to trap incoming photons inside the detector volume until they get absorbed. To achieve stronger coupling between impinging and detected light, the metastructure approach was chosen [6]. Metastructures form a periodic array of small-sized structures on top of a detector mesa that change the surface topography. Depending on the wavelength of the incident radiation, the metastructures can serve as diffraction gratings and Fresnel zone plates or they can give rise to plasmonic coupling effects [6]. All of these effects foster absorption and QE in the detector material. In either case, the stimulated absorption is caused by an increased electric field strength with a strong spatial and spectral dependence. If the electric field distribution inside the detector volume is known, an absorption QE can be calculated. To determine the distribution of the electric field, finite-element-method (FEM) modelling can be employed. The input parameters are the detector geometry, the refractive indexes, and the absorption coefficients of all layers in the relevant spectral range.

The metastructure approach was developed and originally employed for quantum well infrared photo-detectors (QWIPs) [7, 8]. As the approach is not inherently connected to QWIPs, it can be adopted for various detector materials and device concepts in different wavelength ranges. In recent years, the effectiveness of employing metastructures for QE enhancement was successfully demonstrated also for T2SL detectors [6, 9].

2.2. Modelling approach

The metastructures investigated in this study are ring-like in shape and placed periodically on top of a detector mesa. In Fig. 1(a), a schematic of a detector mesa with metastructures is shown.
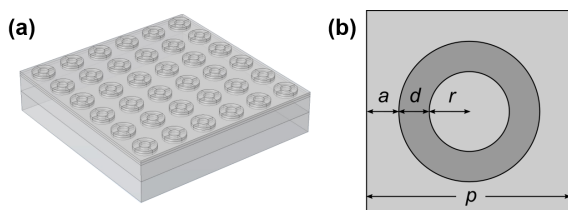

Fig. 1. a: Periodic array of 6×6 ring-like metastructures on top of a detector mesa with a size of 60×60 μm²; b: visualisation of the in-plane metastructure design parameters.

The metastructure geometry is fully defined by the inner and outer ring diameter and the ring height. For modelling purposes, summable dimensions were chosen and four parameters were defined to describe the ring geometry and their periodic spacing: inner ring radius r, ring width d, distance parameter a, and ring height h. The metastructure pitch p in both directions amounts to $p = 2 \cdot (a + r + d)$. Here, Figure 1(b) serves for visualisation.

As mentioned above, the layer structure is required for modelling and metastructure layout. For the initial study, a LWIR T2SL heterojunction diode with a thin absorber layer was chosen because this promises a distinct impact of the metastructures, whereas a spectral smoothing effect is expected for thicker absorbers. The layer structure was designed as follows: GaSb substrate, buffer, etch stop layer, p-type contact, 0.9 μm p-type LWIR absorber, 1.4 μm conduction band matched barrier layer, and n-type contact. After growth, the metastructures can be formed by an initial etch into the contact and barrier layer, which defines the height h. Then, standard diode processing can follow. The experimental confirmation of the modelling results requires substrate removal and characterisation under backside illumination.

2.3. Results

Prior to modelling, the detector geometry was implemented, the structure carefully meshed, and the material parameters that are known from reference samples or literature were assigned. Then, the parameter space was swept semi-automatically by iterating a, d, and r individually or in a combined fashion. Following Ref. 6, $h = 0.5$ μm was predefined.

During the modelling, the spectral QE was calculated for each metastructure parameter set under study. Then, the figure-of-merit for optimisation was quantified. Depending on the addressed application, the QE enhancement can be required at a certain wavelength or over a certain wavelength range, which needs to be considered in advance when defining the figure-of-merit for optimisation.

In Fig. 2, exemplary modelling results are presented for a variation of d with the other three parameters fixed. For all values of d, the QE shows a strong spectral dependence:
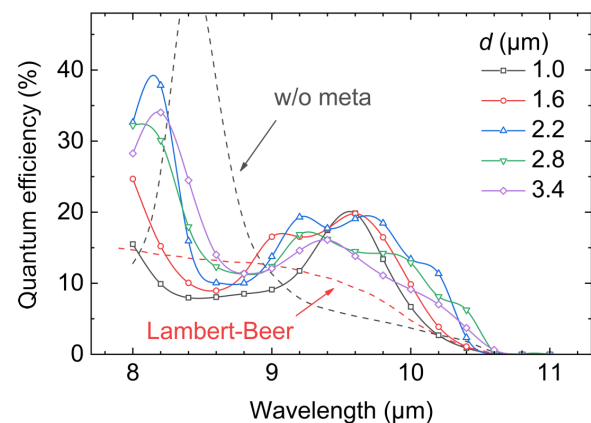

Fig. 2. Spectral QE modelled for different metastructure geometries. In this variation, d changes, while $a = 0.4$ μm, $r = 2.1$ μm, and $h = 0.5$ μm are fixed. The Lambert-Beer law and the modelled reference (flat top without metastructures) that shows an interference effect are also given.

peaks in the 9–10 μm range, a dip around 8.6 μm, and an increase towards 8 μm, which was the lower limit of the investigated wavelength range. In the 9–10 μm range, a maximum QE of 20% is obtained at 9.6 μm for the lower values of *d*.

To assess the influence of the metastructures, two references are presented: first, the Lambert-Beer double-pass QE, which was calculated based on the absorption of a reference T2SL sample, and second, the modelled QE for a flat diode surface without metastructures. The two reference curves differ significantly in shape, because the Lambert-Beer model does not include interference effects. For the modelled reference structure, in the flat top case, such interference effects give rise to the large peak around 8.4 μm and further ones at shorter wavelength. For both references, the QE of 13% at 9 μm decreases monotonically for longer wavelengths. This is in contrast to the modelled curves and highlights that metastructures can substantially increase the detector QE in the LWIR and – in this particular case – at certain wavelengths almost double it.

Considering all modelling and reference curves in the 9–10 μm range, the QE was 20% or less – even with metastructures applied. This owes to the thin absorber layer chosen for this proof-of-principle study and the low LWIR T2SL absorption coefficient. The comparison of modelling and reference curves, however, demonstrates the overall potential to substantially increase the detector QE in the LWIR. The experimental validation of the presented modelling results is pending.

3. MWIR InAs/InAsSb T2SL nBn detectors

3.1. Introduction

During the last decade, InAs/InAsSb (Ga-free) T2SLs have evolved from a fundamentally investigated material for IR detection [10–12], whose potential was demonstrated for different device concepts and IR bands [13–15], into a truly competitive alternative for high performance IR FPAs. Due to its wide acceptance in the field, the nBn device concept [16] is particularly noteworthy in this regard.

At Fraunhofer IAF, we recently started working on InAs/InAsSb T2SLs. In the following, characterisation data of the first MWIR InAs/InAsSb T2SL nBn detectors grown and processed at our institute are presented.

3.2. Epitaxy and processing

An InAs/InAsSb T2SL nBn layer structure was grown by molecular beam epitaxy on 3-inch n-doped GaSb. The layer structure was adapted from Ref. 17 with adjustments to our growth and processing schemes. Non-intentionally doped (n.i.d.) InAs/InAs$_{0.66}$Sb$_{0.34}$ T2SLs with a 12 ML / 4 ML composition form the two n-layers – top contact and absorber – with 16 and 525 periods, respectively. The n-layers are separated by the 120 nm wide AlAs$_{0.085}$Sb$_{0.915}$ barrier layer (B) with a light p-type doping of $1 \cdot 10^{15}$ cm^{-3} (Be). Another 200 superlattice periods – with stoichiometry and composition as described above – form the n-doped bottom contact with $1 \cdot 10^{17}$ cm^{-3} (Te). Additional buffer structures were used between the bottom contact and the substrate. In subsequent standard growth

characterisation, a photoluminescence peak wavelength of 4.66 μm at 10 K and a period length of 5.0 nm measured with high resolution X-ray diffraction were found.

Square mesa detectors of different sizes ranging from 80×80 μm² to 350×350 μm² were fabricated with the subsequently outlined processing scheme. First, detector mesas were realised by inductively coupled plasma etching with an etch depth extending into the bottom contact layer. Then, a dielectric passivation and a metallisation sequence were applied. To perform variable temperature measurements in a lab cryostat, detector chips were cleaved and mounted on dedicated sample carriers that allow for characterisation under backside illumination through the substrate.

3.3. Experimental results

The dark currents of the differently-sized detectors were measured from −1.5 V to 1.5 V at temperatures between 300 K and 77 K. From the characterisation of detectors with different size, it was concluded that the surface current is much lower than the bulk-related currents, hence, sidewall-related dark currents seem negligible in these devices. This finding is in qualitative agreement with Ref. 17, in which the surface of the InAs/InAsSb MWIR T2SLs is described to be n$^+$, implying a self-passivating effect in n-type layers and low surface currents in nBn detectors even without passivation.

In Fig. 3, the dark current density of a 200×200 μm² detector element is presented for temperatures from 296 K to 77 K. At low temperature and low bias, where the resolution limit of the setup is reached, the curve shape indicates a limitation by generation-recombination currents, whereas at elevated bias tunnelling currents dominate. At higher temperatures, the dark current at low bias appears diffusion-limited. To confirm this, the activation energy was determined by an Arrhenius analysis at an intended operating bias of −0.2 V (not shown). The trend suggested a single activation energy above 120 K. Following Ref. 17, the term $j \propto T^3 \exp(-\Delta E/(k_B T))$ was fitted and $\Delta E = 305$ meV was found. This value is close to the bandgap energy supporting the assumption of a diffusion-limited behaviour at elevated temperatures. The activation energy that was deduced in Ref. 17 at the same bias voltage and with the same routine is much lower, whereas the respective dark current densities are higher.
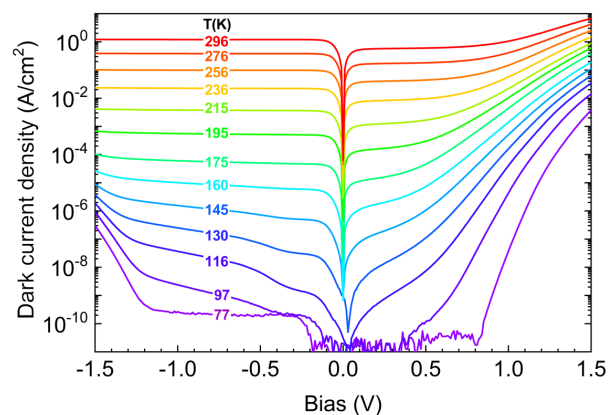

Fig. 3. Dark current density of a MWIR InAs/InAsSb T2SL nBn detector at various temperatures. The detector size is 200×200 μm².

This mainly owes to a notable difference in the bandgap energy that needs to be taken into account for a meaningful comparison. Accordingly, the detector photoresponse was characterised and the results were included for comparison.

The photoresponse of the detectors was measured under backside illumination through the GaSb substrate between 77 K and 180 K with different bias voltages. Figure 4 shows QE spectra that were obtained on the 200×200 µm² detector at -0.4 V. In the inset, the bias-dependence of the QE at different temperatures is presented at $\lambda = 3.7$ µm, a wavelength chosen far from the cut-off. The spectral QE peaks between 0.6 and 0.7 at all temperatures. The temperature dependence of the peak QE is weak. A small QE reduction above 150 K is observable that was attributed to a decreasing hole mobility [17]. The cut-off wavelength exhibits the common redshift related to temperature increase. The inset reveals a turn-on bias of about 0.3 V at 77 K that decreases continuously for higher temperatures. This can be attributed to an unintended valence band offset between absorber and barrier layer [17]. In the investigated temperature range, the device is completely turned on at -0.4 V, so the spectra were presented for this bias voltage. If only the diffusion-limited temperature range above 120 K had been considered, a graphical comparison at -0.2 V would have been possible, too.
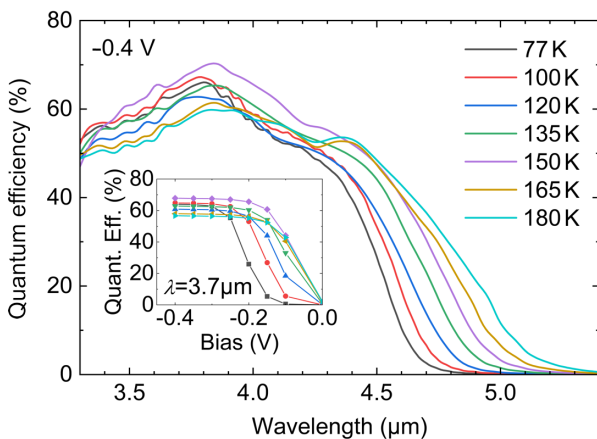

Fig. 4. QE spectra of a MWIR Ga-free nBn detector at different temperatures (-0.4 V bias, 200×200 µm²). Inset: bias-dependence of the QE at different temperatures for $\lambda = 3.7$ µm.

3.4. Analysis and discussion

To compare the performance of IR photodetectors with different cut-off wavelengths, the dark current density is plotted *vs.* the inverse product of cut-off wavelength and operating temperature. Figure 5 shows this dependence for

the detector studied here, the reference from literature [17], other Ga-free MWIR nBn detectors [18, 19], as well as for other published T2SL detector results [20, 21]. All data points shown were either extracted from published QE spectra with the aforementioned cut-off criterion [17–19, 21] or are explicitly specified in the publications for the respective operating bias [20]. For visual benchmarking, also the empirical Rule 07 is given [22].
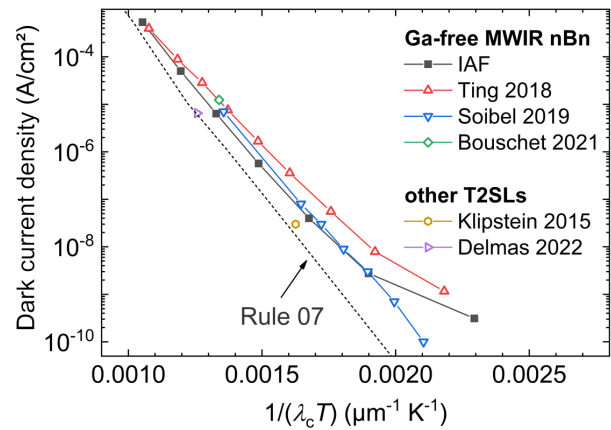

Fig. 5. Dark current density *vs.* inverse product of cut-off wavelength and operating temperature of the investigated detector structure. For comparison, published results of other Ga-free MWIR nBn detectors [17–19], other T2SL detectors [20, 21], and Rule 07 [22] are also plotted.

First, Figure 5 shows that the performance of our detector under study is comparable to the state-of-the-art for MWIR InAs/InAsSb T2SL nBn detectors over a wide temperature range. Only at low temperature a notable deviance exists when compared to Ref. 18, in which the detector was particularly optimised for that range and still appears to be diffusion-limited. All these nBn detector results are approaching Rule 07. Here, it is noteworthy that two groups have published T2SL detector results that are even getting a little closer to the Rule 07 trend line. To sum up, the T2SL detector results shown in Fig. 5 demonstrate the general competitiveness of T2SLs with HgCdTe.

4. MWIR/LWIR dual-band technology

4.1. Introduction

For several defence applications and scenarios, flexible MWIR/LWIR dual-band FPAs are desirable. First, depending on the atmospheric condition, imaging in the MWIR or the LWIR is preferable. Furthermore, as the two channels are sensitive to different signatures of the imaged objects, their combination can provide extended and valuable information. The inherent design flexibility of T2SLs can be utilised to fabricate multi-colour or multi-band IR detector arrays. Accordingly, T2SL-based MWIR/LWIR dual-band imaging technology was demonstrated and is continuously investigated [23–26].

In this paper, the development of bias-switchable MWIR/LWIR dual-band detector arrays with 1280×1024 pixels and 12 µm pitch is discussed. The device structure comprises two back-to-back InAs/GaSb T2SL pPN-diodes for the MWIR and the LWIR, respectively. Regarding the epitaxial layer stack, using two back-to-back diodes is

The results of the photoresponse characterisation, like the peak QE values and the temperature-dependent turn-on, confirm the findings by Ting *et al.* [17]. However, the comparison highlights a noteworthy difference in the detector cut-off wavelength. Taking the cut-off as the wavelength at which the QE has dropped to half its peak value on the longer wavelength side, a cut-off of 4.65 µm at 150 K was found in the data, whereas ~5.3 µm was extracted from the QE spectra in Ref. 17. Hence, further data analysis is required for a proper comparison of the two detector structures.

similar to our MWIR/MWIR dual-colour detector arrays for missile warning. However, the modifications regarding the operation mode, the number of contacts, the hetero-junction device concept, the MWIR/LWIR spectral range, the increased resolution, and the reduced pixel pitch require substantial developments.

The basic design of the back-to-back pPN device concept was based on a previously reported work for either channel [27, 28]. The more challenging modifications are related to the processing technology. To realise a high QE in both channels, a thick epitaxial layer stack and a large fill factor are required. Furthermore, a full pixel reticulation that enables an excellent modulation transfer function performance is intended. For a small pixel pitch of 12 μm, this can only be achieved with steep and narrow etch trenches. The feasibility of such etch trenches was reported by other groups [21, 29]. Previously, we employed etching sequences that lead to V-shaped etch profiles in T2SLs, which are suitable for thinner epilayers or wider pixel pitches and are required for cross-level metallisation lines. Hence, one of the main developments concerned the dry etching technology for steep etch trenches.

4.2. Dry etching for 12 μm pixel pitch

A new process sequence for the realisation of steep etch trenches in T2SLs of several microns in width was developed that allows for small pixel pitch arrays with fully reticulated pixels. During the development process, several hard mask materials, mask dimensions, and sets of ICP etching parameters were investigated and optimised. Finally, a SiO_2 hard mask was chosen.

In Fig. 6, scanning electron microscopy (SEM) images are presented that were taken during the developmental phase. In Fig. 6(a), the close-up demonstrates that full pixel reticulation is reached for a layer width of 8.6 μm. The clear trench between the individual pixels indicates that even a safety margin for process stability is included. This process corresponds to a fill factor of about 70% for the LWIR channel.
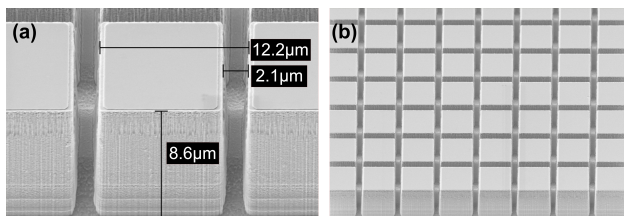

Fig. 6. SEM images of a T2SL MWIR/LWIR dual-band detector array (a: close-up of an individual pixel; b: overview of a 12 μm pitch detector array).

4.3. Dual-band detector characterisation

The layer structure for the back-to-back pPN device structure based on InAs/GaSb T2SLs was grown by molecular beam epitaxy on 4-inch GaSb. Since the development eventually aims at imaging with illumination through a thinned substrate, the LWIR channel was placed on top of the MWIR channel. In the subsequent detector fabrication, the newly developed ICP process for steep etch trenches was included.

The wafer layout included process evaluation chips (PECs), as well as small pitch arrays. For the electrooptical characterisation results presented in the following, the PECs are focused on, as the characterisation data for the arrays were not acquired yet. The characterisation of the PECs was performed in a lab cryostat. For the photoresponse characterisation, the devices on the PECs were illuminated through a frontside processing window.

In Fig. 7, the dark current density of a bias-switchable MWIR/LWIR dual-band detector at 77 K is presented. In the inset, a scanning electron microscopy image of the 200×110 μm²-sized detector with frontside processing window is shown. The graph reveals that depending on the applied voltage, one of the two channels is biased in reverse and, hence, active. In both channels, at low bias, the current-voltage dependence is week, whereas at elevated bias, the current increases steeply due to tunnelling currents. At a typical operating bias of 250 mV, the current density is $6.1 \cdot 10^{-9}$ A/cm² for the MWIR channel and $5.3 \cdot 10^{-4}$ A/cm² for the LWIR channel. For rating these dark current densities, it is noteworthy that photoluminescence yielded 4.9 μm and 11.3 μm as bandgap equivalent wavelength at 10 K. For operation at 77 K, these dark current densities allow for a 300 K background-limited operation with f/2-optics.
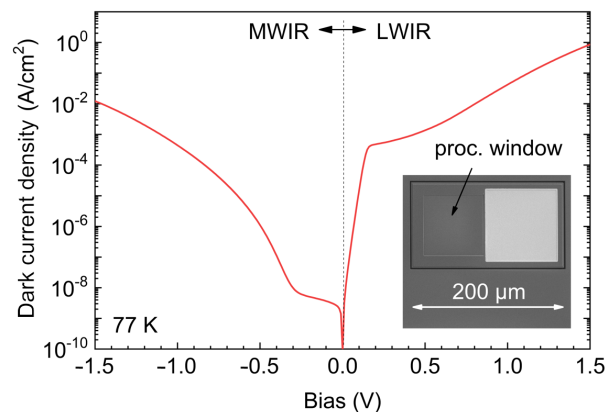

Fig. 7. Dark current density of a MWIR/LWIR dual-band detector for bias-switchable operation at 77 K. Inset: top-view SEM image of the 200×110 μm²-sized detector with a frontside processing window.

In Fig. 8, the bias-dependent photocurrent density is presented that was measured on this dual-band detector with a 1100 °C blackbody, a mechanical chopper wheel, and a lock-in amplifier. To discriminate the two channels, spectral filters for the MWIR (4.4–5.5 μm) and the LWIR (7.5–11.5 μm) were employed. In both channels, the photosignal exhibits a turn-on voltage of 250 mV. This turn-on behaviour indicates that the device layout has not been optimised yet. A lower turn-on voltage would allow for a reduction of the operating bias and the dark current. Hence, the device layout will be optimised by structure design in the ongoing development. Furthermore, in both channels, the photosignal decreases slightly at higher bias, which is poorly understood to date and will be investigated deeper in the future.

In the photocurrent curves, a photosignal is notable also when the LWIR channel is active and the MWIR filter applied. This is not a signature of spectral crosstalk, that needs to be corrected by changing the structure design but
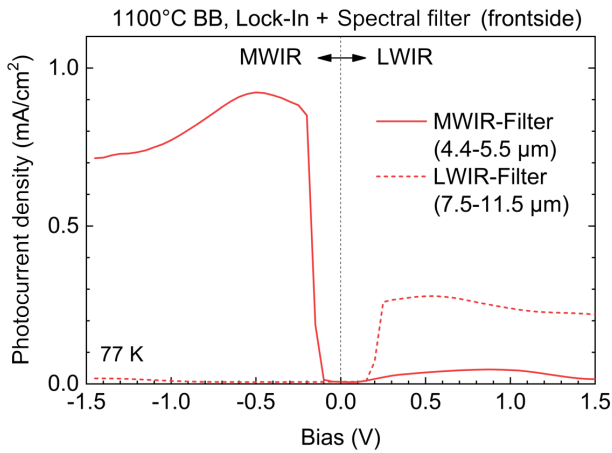
Fig. 8. Photocurrent density of the MWIR/LWIR dual-band detector at 77 K. The measurement was performed under frontside illumination with a 1100°C blackbody source, colour filters, a mechanical chopper wheel, and a lock-in amplifier. The spectral width of the filters is indicated, respectively.

owes to the frontside illumination of the dual-band detector. In this case, MWIR radiation inevitably generates a photosignal in the LWIR T2SL, because the impinging radiation passes this lower bandgap channel first. The estimates on the device performance in the final configuration under backside incident radiation suggest a properly operating bias-switchable MWIR/LWIR dual-band detector.

5.   Conclusions

In this paper, three different developments in the field of T2SL detector research at Fraunhofer IAF were reported. These developments are performed whilst considering the common trends in the research field that aim at: improving the detector response, reducing the dark current density, and/or increasing the detector array resolution/shrinking the pixel size.

In the first part, an approach to increase the QE in LWIR T2SL detectors was described. The approach consists of utilising metastructures that enable a conceptually different coupling of the incident radiation to the detector. By giving rise to diffractive and plasmonic effects, the metastructures impact the electric field distribution inside the detector volume, which can be determined by finite-element modelling. For different metastructures, whose layout was altered semi-automatically, the electric field distribution in spatial and spectral dependence was modelled inside a T2SL detector with a 0.9 μm thick absorber layer. For each metastructure parameter set, based on the modelling results, a spectral QE was calculated. With this approach, several parameter sets were identified that should enable a substantial increase in QE in LWIR T2SL detectors. For the structure under study, the modelling results indicate a doubling of the QE in the 9–10 μm range. The experimental confirmation of these modelling results is currently pending. In future developments, a transfer of the know-how established in this proof-of-principle study to other layer structures and device concepts is intended.

In the second part, characterisation data of the first MWIR InAs/InAsSb T2SL nBn detectors fabricated at Fraunhofer IAF were presented. The device structure was adapted from Ting *et al.* [17], whose results served as reference point for performance evaluation. The investigated detectors displayed very low dark current densities that were dominated by the bulk and diffusion-limited above 120 K. The corresponding QE was above 60% over the 77–180 K temperature range. Qualitatively, most of the characterisation results confirmed Ref. 17. However, because the observed cut-off wavelength differed from the reference, it was corrected to also obtain a meaningful quantitative comparison. Consequently, it was found that the investigated detectors perform comparably to the state-of-the-art in this field, which is approaching the empirical Rule 07. A potential to further improve the device design was identified during the data analysis, which will be addressed in future developments.

The third and last part of the paper was devoted to research on MWIR/LWIR dual-band imaging technology with 1280×1024 pixel resolution at 12 μm pitch. For the device design InAs/GaSb T2SLs are utilised in a back-to-back pPN heterojunction diode concept. To realise a full pixel reticulation and a high QE, an ICP etching process was developed. The final process allows for steep etch trenches and a high fill factor even in T2SL layer stacks of 8.6 μm in width which was demonstrated by SEM images. Finally, a fill factor of about 70% was achieved in a homogeneous process. The potential for the bias-switchable dual-band operation mode was demonstrated by the PEC-based detector characterisation. For 77 K and ±250 mV bias, dark current densities of $6.1 \cdot 10^{-9}$ A/cm² in the MWIR and $5.3 \cdot 10^{-4}$ A/cm² in the LWIR were obtained that allow for 300 K background-limited operation with f/2-optics. The corresponding photocurrent measurement, that was performed under frontside illumination, suggested the suitability for MWIR/LWIR dual-band detection in the intended operation mode. In the future, hybridised detector arrays with removed substrates will be characterised under backside illumination. Besides, an optimisation of the device design is intended. This concerns the dark current density in the LWIR channel, where potential for increasing the operating temperature is given, as well as a reduction of the observed turn-on voltage. Eventually, the aim is to realise T2SL-based high-performance MWIR/LWIR dual-band imaging technology.

References

[1] Ting, D. Z. *et al*. Antimonide type-II superlattice barrier infrared detectors. *Proc. SPIE* **10177**, 101770N (2017). https://doi.org/10.1117/12.2266263

[2] Hill, C. J. *et al*. The VISTA industrial consortium: structure and accomplishments of a government-industry development partnership. *Proc. SPIE* **12107**, 121070P (2022). https://doi.org/10.1117/12.2618983

[3] Fuchs, F. *et al*. High performance InAs/Ga$_{1-x}$In$_x$Sb superlattice infrared photodiodes. *Appl. Phys. Lett.* **71**, 3251 (1997). https://doi.org/10.1063/1.120551

[4] Herres, N. *et al*. Effect of interfacial bonding on the structural and vibrational properties of InAs/GaSb superlattices. *Phys. Rev. B* **53**, 15688 (1996). https://doi.org/10.1103/PhysRevB.53.15688

[5] Rehm, R. *et al*. Dual-colour thermal imaging with InAs/GaSb superlattices in mid-wavelength infrared spectral range. *Electron. Lett.* **42**, 577–578 (2006). https://doi.org/10.1049/el:20060878

[6] Choi, K.-K. Metastructures for VLWIR SLS detectors. *Proc. SPIE* **11407**, 114070K (2020). https://doi.org/10.1117/12.2555954

[7] Choi, K.-K. *et al*. Electromagnetic modeling of quantum well infrared photodetectors. *IEEE J. Quantum. Electron.* **48**, 384–393 (2012). https://doi.org/10.1109/JQE.2011.2175706

[8] Choi, K.-K. *et al*. Small pitch resonator-QWIP detectors and arrays. *Infrared Phys. Technol.* **94**, 118–125 (2018). https://doi.org/10.1016/j.infrared.2018.09.006

[9] Gunapala, S. D. *et al*. T2SL meta-surfaced digital focal plane arrays for Earth remote sensing applications. *Proc. SPIE* **11129**, 111290C 2019). https://doi.org/10.1117/12.2533477

[10] Steenbergen, E. *et al*. Significantly improved minority carrier lifetime observed in a long-wavelength infrared III-V type-II superlattice comprised of InAs/InAsSb. *Appl. Phys. Lett.* **99**, 251110 (2011). https://doi.org/10.1063/1.3671398

[11] Lackner, D. *et al*. Growth of InAsSb/InAs MQWs on GaSb for mid-IR photodetector applications. *J. Cryst. Growth* **311**, 3563–3567 (2009). https://doi.org/10.1016/j.jcrysgro.2009.04.027

[12] Lackner, Di. *et al*. Strain balanced InAs/InAsSb superlattice structures with optical emission to 10 µm. *Appl. Phys. Lett.* **95**, 081906 (2009). https://doi.org/10.1063/1.3216041

[13] Kim, H.S. *et al*. Long-wave infrared nBn photodetectors based on InAs/InAsSb type-II superlattices. *Appl. Phys. Lett.* **101**, 161114 (2012). https://doi.org/10.1063/1.4760260

[14] Hoang, A. M., Chen, G., Chevallier, R., Haddadi, A. & Razeghi, M. High performance photodiodes based on InAs/InAsSb type-II superlattices for very long wavelength infrared detection. *Appl. Phys. Lett.* **104**, 251105 (2014). https://doi.org/10.1063/1.4884947

[15] Haddadi, A. M., Chen, G., Chevallier, R., Hoang, A. M & Razeghi, M. InAs/InAs$_{1-x}$Sb$_x$ type-II superlattices for high performance long wavelength infrared detection. *Appl. Phys. Lett.* **105**, 121104 (2014). https://doi.org/10.1063/1.4896271

[16] Maimon, S. & Wicks, G. W. nBn detector, an infrared detector with reduced dark current and higher operating temperature. *Appl. Phys. Lett.* **89**, 151109 (2006). https://doi.org/10.1063/1.2360235

[17] Ting, D. *et al*. Mid-wavelength high operating temperature barrier infrared detector and focal plane array. *Appl. Phys. Lett.* **113**, 021101 (2018). https://doi.org/10.1063/1.5033338

[18] Soibel, A. *et al*. Mid-wavelength infrared InAsSb/InAs nBn detectors and FPAs with very low dark current density. *Appl. Phys. Lett.* **114**, 161103 (2019). https://doi.org/10.1063/1.5092342

[19] Bouschet, M. *et al*. Influence of pixel etching on electrical and electro-optical performances of a Ga-free InAs/InAsSb T2SL barrier photodetector for mid-wave infrared imaging. *Photonics* **8**, 194 (2021). https://doi.org/10.3390/photonics8060194

[20] Klipstein, P. C. XBnn and XBpp infrared detectors. *J. Cryst. Growth* **425**, 351–356 (2015). https://doi.org/10.1016/j.jcrysgro.2015.02.075

[21] Delmas, M. *et al*. HOT SWaP and HD detectors based on Type-II superlattices at IRnova. *Proc. SPIE* **12107**, 121070R (2022). https://doi.org/10.1117/12.2618752

[22] Tennant, W. E. ''Rule 07'' Revisited: still a good heuristic predictor of p/n HgCdTe photodiode performance? *J. Electron. Mater.* **39**, 1030–1035 (2010). https://doi.org/10.1007/s11664-010-1084-9

[23] Haddadi, A., Chevallier, R., Chen, G., Hoang, A. M. & Razeghi, M. Bias-selectable dual-band mid-/long- wavelength infrared photodetectors based on InAs/InAs$_{1-x}$Sb$_x$ type-II superlattices. *Appl. Phys. Lett.* **106**, 011104 (2015). https://doi.org/10.1063/1.4905565

[24] Plis, E. *et al*. Dual-band pBp detectors based on InAs/GaSb strained layer superlattices. *Infrared Phys. Technol.* **59**, 28–31 (2013). https://doi.org/10.1016/j.infrared.2012.12.005

[25] Ariyawansa, G. *et al*. Design and modeling of InAs/GaSb type II superlattice based dual-band infrared detectors. *J. Appl. Phys.* **111**, 073107 (2012). https://doi.org/10.1063/1.3702581

[26] Gurga, A. R., Nosho, B. Z., Terterian, S., Wang, S. & Rajavel, R. D. Dual-band MWIR/LWIR focal plane arrays based on III-V strained-layer superlattices. *Proc. SPIE* **10624**, 1062400 (2018). https://doi.org/10.1117/12.2309720

[27] Rehm, R. *et al*. Type-II superlattice infrared detector technology at Fraunhofer IAF. *Proc. SPIE* **9819**, 98190X (2016). https://doi.org/10.1117/12.2223887

[28] Schmidt, J., Rutz, F., Wörl, A., Daumer, V. & Rehm, R. Low dark current in mid-infrared type-II superlattice heterojunction photodiodes. *Infrared Phys. Technol.* **85**, 378–381 (2017). https://doi.org/10.1016/j.infrared.2017.08.001

[29] Huang, E., Nguyen, B.-M., Hoffman, D., Delaunay, P.-Y. & Razeghi, M. Inductively coupled plasma etching and processing techniques for type-II InAs/GaSb superlattices infrared detectors toward high fill factor focal plane arrays. *Proc. SPIE* **7222**, 72220Z (2009). https://doi.org/10.1117/12.810030